Gravity effects on triple flames: Flame structure and flow instability

Riccardo Azzoni, Stefano Ratti, Ishwar K. Puri, and Suresh K. Aggarwal[a)]
University of Illinois at Chicago, Department of Mechanical Engineering (M/C 251), 842 W. Taylor St. RM 2039 ERF, Chicago, Illinois 60607-7022

(Received 2 April 1999; accepted 9 July 1999)

A fundamental difference between a partially premixed flame and an equivalent premixed (or nonpremixed) flame pertains to the existence of multiple synergistically coupled reaction zones. A ''triple flame'' is a type of partially premixed flame that contains a fuel-rich premixed reaction zone, a fuel-lean premixed reaction zone, and a nonpremixed reaction zone. The objective of this investigation is to examine gravity effects on the flame structure and flow instabilities related to partially premixed triple flames. (An earlier investigation by us dealing with gravitational effects on partially premixed double flames essentially considered steady 0- and 1-g flames.) A detailed numerical model is employed to simulate a methane-air triple flame established on a slot burner. A relatively detailed mechanism involving both C_1- and C_2-containing species and 81 elementary reaction steps is used to represent the CH_4-air chemistry. Validation of the computational model is provided through a comparison of predictions with nonintrusive measurements. The results indicate that the overall triple flame structure is determined by interactions between the three reaction zones, and can be controlled by changing the mixture velocity, equivalence ratio, and gravitational acceleration. While the inner rich premixed reaction zone is weakly affected by gravity, the central nonpremixed and outer lean premixed reaction zones exhibit significant differences at 0 and 1 g. For 0 g flames, these two reaction zones move away from the centerline compared to the corresponding 1 g flames, since the entrainment of the lean outer flow is reduced in the absence of buoyant advection. Velocity vectors outside the lean premixed zone are directed away from the centerline due to flow dilatation in a 0 g flame, whereas they are directed towards the centerline due to the buoyancy-induced entrainment that occurs in a corresponding 1 g flame. Consequently, there is an increased physical separation and reduced heat and mass transport between the three reaction zones of the 0 g flame. The nonpremixed reaction zone height decreases due to the increase in residence time at 0 g. The reduced advection and (transport) at 0 g results in a flame that is less compact and has thicker reaction zones and which, therefore, is more sensitive to flow or stoichiometry perturbations. The flame structure and the interactions between the three reaction zones are found to be well-represented in terms of a modified conserved scalar ξ. A fundamental difference between the 0 and 1 g triple flames is due to their transient behavior and markedly different response to changes in the coflow velocity. Our simulations indicate the presence of a shear-induced convective instability and a buoyancy-induced global instability in laminar triple flames that depend upon the magnitude of coflow velocity and gravitational acceleration. The outer premixed reaction zone of 0 g flames exhibits a hitherto unreported weak oscillatory behavior at higher coflow rates that is related to a Kelvin–Helmholtz instability of the momentum shear layer. The instability in the 0 g flame is confined to the outer premixed zone. In contrast, decreasing the coflow velocity at 1 g causes a well-organized flickering of the outer reaction zone that can affect all three reaction zones. The flickering frequency is relatively insensitive to changes in the coflow velocity, as both computed and measured frequencies are found to be in a narrow range of 9–12 Hz. However, the flickering amplitude exhibits strong sensitivity to the coflow velocity as it is reduced to a value smaller than the inner jet velocity, and becomes noticeably large causing oscillations in all three reaction zones. There is a good agreement between the predicted and measured dynamics of the flickering 1 g flames. © *1999 American Institute of Physics.* [S1070-6631(99)00411-0]

INTRODUCTION

Partially premixed flames are hybrid flames containing multiple reaction zones. These flames are of fundamental importance to the phenomena of nonpremixed flame stabilization and liftoff, spray combustion, and localized extinction and reignition in turbulent flames. A double flame[1–3] containing a fuel-rich premixed reaction zone that synergistically interacts with a nonpremixed reaction zone is an example of a partially premixed flame. A triple flame[4–6] that contains three reaction zones offers another example. A triple flame contains a fuel-rich premixed zone, a fuel-lean premixed zone, and a nonpremixed reaction zone. We will discuss such a flame, in which the two premixed reaction zones form exterior wings and the nonpremixed reaction

a)Author to whom correspondence should be addressed. Electronic mail: ska@uic.edu

zone is established in between these two wings (in the region where excess fuel and oxidizer from the rich and lean premixed reaction zones, respectively, mix in stoichiometric proportion). The overall flame structure is determined by the interactions between these three reaction regions, and can be controlled by changing the various reactant velocities and equivalence ratios.

A fundamental difference between a partially premixed flame and an equivalent premixed or nonpremixed flame pertains to the existence of multiple synergistically coupled reaction zones. The structure of partially premixed flames is determined by the interactions that arise among these zones due to the synergy between the thermochemistry and the heat and mass transport. For example, in a methane–air triple flame the inner rich premixed reaction zone provides CO and H_2, which serve as ''intermediate fuels,'' and excess methane to the nonpremixed zone, whereas the latter supplies heat and radical species (H and OH) to both the inner and outer zones.[6] The outer zone in turn provides excess O_2 and oxygen atoms to the nonpremixed reaction zone. The interactions between the various reaction zones occur due to the advection and diffusion of both heat and mass. These effects are strongly influenced by flow dilation and gravity, as well as flame curvature and differential diffusion. In a normal-gravity partially premixed flame, the flow dilatation due to the heat release in the inner zone directs the velocity vectors towards the nonpremixed zone (away from the centerline), whereas buoyancy has an opposite consequence.[7] A similar effect occurs in the region between the nonpremixed and outer premixed zones. Therefore, the physical separation between the reaction zones is reduced so that the topography of the nonpremixed and outer premixed zones is modified in the absence of gravity. The stretch rate experienced by these zones is also altered.

We have recently examined the effects of flow dilatation and buoyancy on the structure of a steady two-dimensional partially premixed methane-air double flame[7] (recall that a double flame contains two reaction zones, one which is a rich premixed reaction zone, and the other a nonpremixed reaction zone). In that flame, methane was partially oxidized to form CO and H_2 in the inner premixed reaction zone and these species were transported to the outer nonpremixed zone where they were oxidized to form CO_2 and H_2O. The outer zone in turn supplied heat and radical species such as OH and H-atoms to the inner zone. For the investigated conditions, we found the inner premixed zone to be relatively unaffected by either flow dilatation or buoyancy, since these effects were confined to the post-flame region. The structure of the nonpremixed zone was, however, strongly influenced by both flow dilatation and buoyancy. The flow dilatation pushed the outer nonpremixed zone further outward (away from the centerline), while buoyant convection had the opposite effect. Consequently, the absence of gravity resulted in an increased separation between the two reaction zones. The 0 g nonpremixed zone was spatially larger and thicker compared to the corresponding 1 g flame, since transverse diffusive transport were enhanced relative to advection in zero gravity.

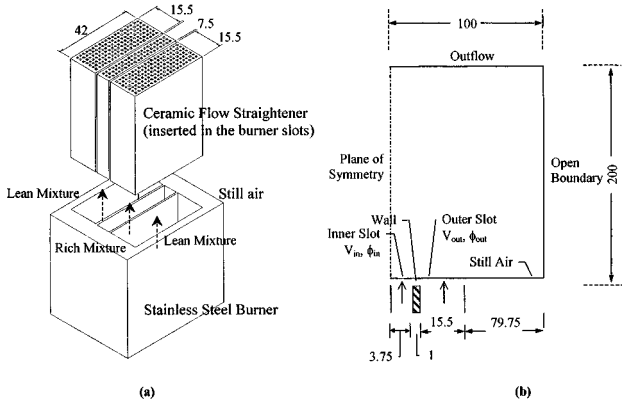

FIG. 1. Schematic diagram of (a) the burner, and (b) the computational domain and boundary conditions. Dimensions are in units of mm.

The objective of this investigation is to examine gravity effects on the structure of a partially premixed triple flame. In contrast to a double flame in which gravity mainly affects the outer nonpremixed reaction zone, in the triple flame buoyancy is expected to influence both the outer lean premixed and the central nonpremixed reaction zones. This in turn can influence the inner premixed reaction zone. The outer premixed zone may also mitigate the influence of gravity on the nonpremixed zone by providing a shield against the buoyant convection. Furthermore, the outer zone of a triple flame, being a region of lean premixed combustion, is expected to be more prone to inherent flow and combustion instabilities as compared to a double flame.

NUMERICAL MODEL

Our numerical model simulates a triple flame established on a Wolfhard–Parker slot burner (that is schematically illustrated in Fig. 1). A rich mixture is introduced from the inner slot and a lean mixture is introduced from the two symmetric outer slots. This configuration has been used by us in recent investigations[3,6,7] in which the numerical results were validated by a comparison with nonintrusive measurements. The experimental diagnostics involved chemiluminescent emission imaging of excited C_2^* radicals,[3,6,7] holographic interferometry temperature measurements,[7] and particle image velocimetry (PIV)[3] and laser Doppler velocimetry (LDV)[7] velocity measurements.

The numerical model is based on the solution of time-dependent governing equations for a two-dimensional reacting flow. Using Cartesian coordinates (x,y), these equations can be written in the form

$$\frac{\partial(\rho\psi)}{\partial t}+\frac{\partial(\rho u\psi)}{\partial x}+\frac{\partial(\rho v\psi)}{\partial y}$$

$$=\frac{\partial}{\partial x}\left(\Gamma^{\phi}\frac{\partial\psi}{\partial x}\right)+\frac{\partial}{\partial y}\left(\Gamma^{\phi}\frac{\partial\psi}{\partial y}\right)+S^{\phi},$$

where ρ denotes density, and u and v, respectively, represent the transverse (x) and axial (y) velocity components. The general form of the equation represents either of the mass,

momentum, species, or energy conservation equations, depending upon the variable used in place of ψ. The gravitational acceleration term is included in the axial momentum equation. The transport coefficient Γ^{ϕ} and the source terms S^{ϕ} appearing in the governing equations are provided in Refs. 7 and 8. The set of governing equations is completed by introducing the global species conservation equation and the state equation $p=\rho TR_u\Sigma_1^N Y_i/M_i$, where R_u represents the universal gas constant, T the temperature, and M_i the molecular weight of ith species. The thermodynamic and transport properties appearing in the above equations are considered to be temperature and species dependent. First, the viscosity and thermal conductivity of the individual species are estimated based on Chapman–Enskog collision theory, following which those of the mixture are determined using the Wilke semiempirical formulas. Chapman–Enskog theory and the Lennard-Jones potentials are used to estimate the binary-diffusion coefficient between each species and nitrogen.[8] A relatively detailed 24-species, 81-step mechanism involving both C_1- and C_2-containing species is used to represent the CH_4–air chemistry.[9]

The computational domain is bounded by the symmetry plane and an outflow boundary in the transverse direction, and by the inflow and another outflow boundary in the axial direction. Symmetric conditions are applied at the left boundary, whereas the right boundary is treated as a free surface. At the inflow boundary, except for the wall where no-slip boundary conditions are imposed, uniform velocity profiles are assumed for both the inner fuel-rich and outer fuel-lean streams. The temperature and species mass fraction profiles are also assumed to be uniform at the inflow boundary. The flow variables at the outflow boundary are obtained using an extrapolation procedure with weighted zero- and first-order terms. The main criterion used in selecting the weighting functions is that the flow should exit the outflow boundary without being distorted. In addition, the outflow boundaries in both directions are located sufficiently far from the respective inflow and symmetric boundaries so that the propagation of boundary-induced disturbances is minimized. The boundary conditions are indicated in Fig. 1.

The computational model is based on an algorithm developed by Katta *et al.*[8] An implicit algorithm is employed to solve the unsteady gas-phase equations. The governing equations are integrated by using a ''finite control volume'' approach with a staggered, nonuniform grid system (131×88). Grid lines are clustered near the flame surfaces to resolve the steep gradients of the dependent variables. An iterative ADI (Alternating Direction Implicit) technique is used for solving the resulting (N_s+3) sets of algebraic equations. A stable numerical-integration procedure is achieved by coupling the species and energy equations through the chemical-reaction source terms. At every time step, the pressure field is calculated by solving the pressure Poisson equations at all grid points simultaneously and utilizing the LU (Lower and Upper diagonal) matrix-decomposition technique.[3,8,10]

RESULTS AND DISCUSSION

Further validation of the computational model for a representative triple flame established under 1 g conditions is provided through a comparison of predictions with measurements. Figure 2(a) presents a comparison between the computed volumetric heat release rates (left) with the experimentally measured C_2^*-chemiluminescence intensities.[6,11] The excited C_2^* free radical species is considered to be a good indicator of the reaction zone in the fuel-rich regions of flames, in which its light intensity varies linearly with the volumetric heat release.[6]

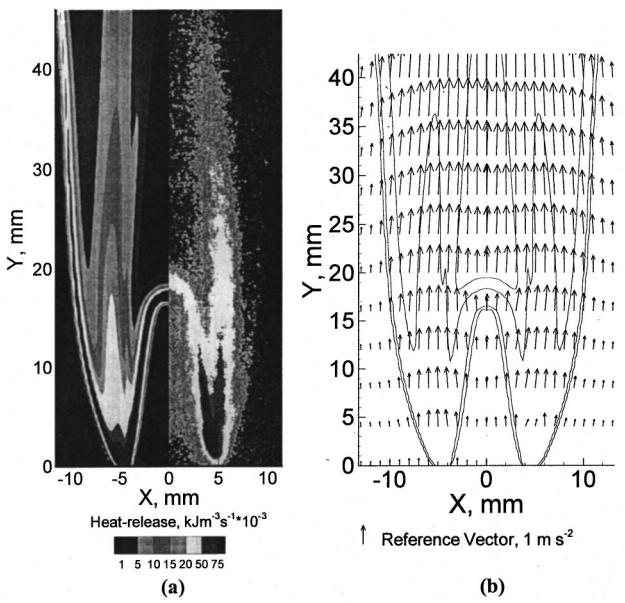

FIG. 2. (a) Comparison between the computed volumetric heat release rates (left) and an experimentally obtained C_2^*-chemiluminescence image (right) for a 1 g flame established at $\phi_{in}=1.8$, $\phi_{out}=0.35$, $v_{in}=0.3\ \mathrm{m\ s^{-1}}$, $v_{out}=0.3\ \mathrm{m\ s^{-1}}$, $\phi_{overall}=0.6$. The experimental image has been normalized by multiplying each pixel intensity by a constant value, which is the ratio of the maximum heat release rate to the maximum pixel intensity. (b) Comparison between the predicted (left) and measured velocity vectors for the same flame.

The C_2^*-chemiluminescence images were obtained using a 513×480 pixel intensified and gated solid-state camera (ITT F4577). A narrow wavelength interference filter (470 ± 10 nm) was employed to detect the emission occurring at 473 nm due to the (1,0) C_2 Swan band.[12] A background image was subtracted from the raw images to correct for noise. Since the chemiluminescence images are directly proportional to the C_2^* formation rate, they, therefore, serve as a qualitative rate measure of the flame chemistry.[13] We observe from Fig. 2(a) that the predicted flame shape is in excellent agreement with the spatial profile of the measured chemiluminescence intensity. While the locations of the rich premixed and the nonpremixed reaction zones are in agreement, the lean premixed reaction zone has a weaker chemiluminescent intensity than the predictions indicate. This is due to the fact that C_2^* radicals are relatively weaker in the outer lean premixed reaction zone than in richer regions.[6] This difference can be attributed to the dominant reaction pathways that are different in the lean and rich premixed regions.[6] Perhaps, the OH chemiluminescence should be employed to capture the reaction zone in the lean premixed region.

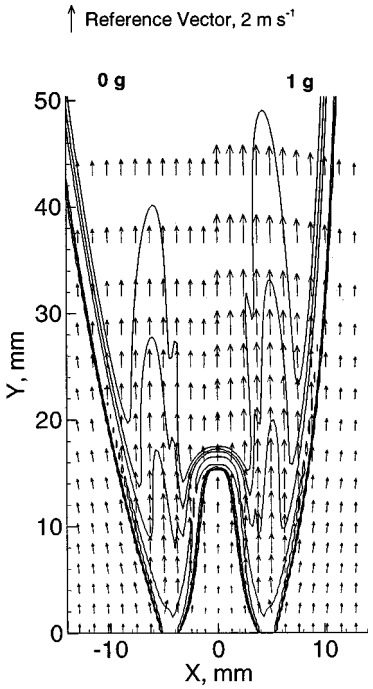

FIG. 3. Comparison of 0 g (left) and 1 g (right) triple flames in terms of the heat release rate (in units of $kJ\,m^{-3}\,s^{-1}$) contours and velocity vectors for reference flames corresponding to the stoichiometric and flow conditions: $\phi_{in}=1.8$, $\phi_{out}=0.38$, $v_{in}=0.3\,m\,s^{-1}$, $v_{out}=0.7\,m\,s^{-1}$, $\phi_{overall}=0.5$.

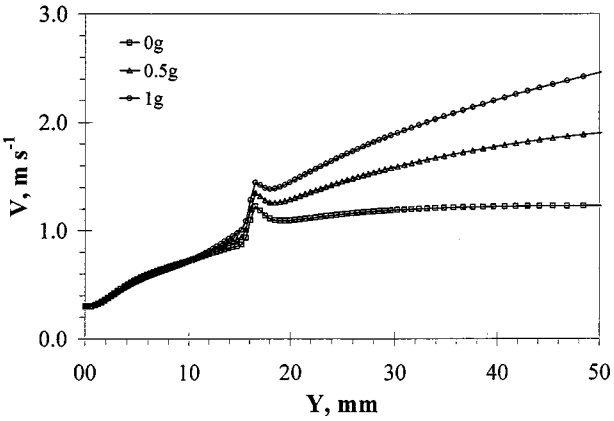

FIG. 4. Axial velocity profiles for the reference conditions of Fig. 3, but at 0, 0.5, and 1 g.

Figure 2(b) presents a comparison between the predicted (left) and measured (right) velocity vectors for the same flame. The predicted heat release rates are also shown so that the locations of the three reaction zones can be identified. The measured velocity vectors are obtained using LDV, details of which are presented elsewhere.[6] There is good quantitative agreement between the measured and predicted velocities. The heat release produces dilatation effects normal to the inner and outer premixed reaction zones. This directs the velocity vectors away from the centerline, which is apparent downstream of the inner reaction zone near the base and near the nonpremixed zone in Fig. 2(b). Buoyancy effects entrain the oxidizer from the lean outer flow and transport it to the nonpremixed reaction zone and, consequently, the velocity vectors turn towards the centerline. These results are in accord with previous predictions regarding gravitational effects on partially premixed flames containing two reaction zones.[7]

Effect of gravity on the global triple flame structure

Figure 3 depicts the global structure of a representative triple flame established under 0 g (left) and 1 g (right) conditions at an overall equivalence ratio $\phi=0.5$. The global equivalence ratio is based on the total mass flow rates of fuel and air in both the inner and outer streams. Other conditions for this case are $\phi_{in}=1.8$, $\phi_{out}=0.38$, $v_{in}=0.3\,m\,s^{-1}$, $v_{out}=0.7\,m\,s^{-1}$, where ϕ_{in} and ϕ_{out} represent the equivalence ratios in the inner and outer streams, respectively, and v_{in} and v_{out} respectively, represent the inner and outer stream velocities. We will hereafter refer to these two (0 and 1 g) flames as the reference flames. The Froude number ($Fr=v_{in}/(gL)^{1/2}$, where $v_{in}=0.3\,m\,s^{-1}$, $g=9.81\,m\,s^{-2}$, and $L=0.0075\,m$ for the 1 g reference flame has a value of 1.11.

The predicted velocity vectors and heat release rate contours are presented for the 0 and 1 g flames in Fig. 3. The three reaction zones are readily identified from the heat release rate contours, which show that the central nonpremixed reaction zone separates an inner fuel-rich premixed zone and an outer fuel-lean premixed zone. The inner rich premixed reaction zone is virtually unaffected by gravity, but both the central nonpremixed and outer lean premixed reaction zones exhibit significant differences at 0 and 1 g. At 0 g, locations of the reaction zones move away from the centerline as compared to the corresponding 1 g flames, since the entrainment of the lean outer flow towards the centerline is considerably reduced due to the absence of buoyant advection.

The presence of gravity increases the nonpremixed reaction zone height, since buoyant acceleration and advection decreases the residence time available to the flow to move through the domain. The enhanced buoyant advection is illustrated in Fig. 4, which presents the centerline velocity with respect to the axial displacement for three 0, 0.5, and 1 g flames, established at the reference flow and stoichiometry conditions. At 0 g the nonpremixed reaction zone is, consequently, less stretched, and has a less intense tip due to the reduction in transport and, therefore, chemical activity. Heat and mass transport is also reduced due to the larger physical separation between this and other reaction zones in the absence of gravity. These observations regarding the nonpremixed reaction zone are consistent with the results of our previous investigation that pertains to gravity effects on partially premixed double flames.[7]

As we have mentioned earlier, gravity modifies the transport-induced interactions between the various reaction zones. For example, the flow dilatation downstream of the inner premixed and central nonpremixed zones directs the velocity vectors toward the outer premixed zone (i.e., away from the centerline), whereas buoyant advection has an opposite effect. In addition, the velocity vectors outside the lean premixed zone are directed away from the centerline due to flow dilatation in the 0 g flame, whereas they are directed towards the centerline due to the buoyancy-induced

entrainment that occurs in the 1 g flame. Consequently, the presence of gravity decreases the spatial separation between the central nonpremixed and outer premixed zones, thereby further enhancing the synergism between the two regions.

Effects of equivalence ratio and coflow velocity

The effect of stoichiometry on the global flame structure at both 0 and 1 g is illustrated in Fig. 5, which presents heat release rates and velocity vectors for three cases. The equivalence ratios for these cases are: (a) $\phi_{in}=1.6$ and $\phi_{out}=0.40$, (b) $\phi_{in}=1.8$, $\phi_{out}=0.38$, and (c) $\phi_{in}=2.1$ and $\phi_{out}=0.36$. For all these cases the global equivalence ratio is 0.5, and the velocities in the inner and outer streams (that are related to the global residence time) are 0.3 and 0.7 $m\,s^{-1}$, respectively. Case (b) corresponds to the reference conditions.

For all of the cases the three reaction zones can be clearly distinguished: A central nonpremixed reaction zone is located between an inner rich premixed zone and an outer lean premixed zone. The height of the inner reaction zone increases as the equivalence ratio of the inner stream is raised. The richer the mixture in the inner stream, the longer it takes for the fuel consumption reactions to be complete. Therefore, since the global residence time is held constant in the three cases, the variation of the inner reaction zone height with ϕ_{in} is due to differences in the chemical reaction time. The central nonpremixed reaction zone establishes itself at locations where stoichiometric conditions exist. Consequently, its height adjusts to that of the inner premixed zone, and this length increases as ϕ_{in} is raised.

The outer lean premixed zone is affected relatively mildly upon varying the equivalence ratios. This zone bends further toward the centerline and moves closer to the nonpremixed reaction zone as ϕ_{out} decreases due to the increase in the chemical reaction time in the outer zone. The heat release rates appear to be of the same order of magnitude in the three reaction zones near the flame base, but are much weaker at the tip of the nonpremixed reaction zone, since fuel is relatively scarce at that location.

The inner premixed reaction zone does not appear to be affected by gravity for the three cases presented in Fig. 5. However, gravity has a significant influence on both the central nonpremixed and outer premixed reaction zones in a similar manner to the case presented in Fig. 3. The locations of these reaction zones move away from the centerline at 0 g as compared to the respective 1 g flames, since both advection and entrainment are reduced in the absence of buoyancy. Again, due to the reduced advective transport, the nonpremixed zone height decreases in the absence of gravity. In general, both the qualitative and quantitative effects of gravity on the triple flame structure are similar over the range of equivalence ratios that we have investigated.

For all three cases discussed in Fig. 5, the outer premixed reaction zone of the 1 g flames is steady, whereas that of the 0 g flames exhibits a weak oscillatory behavior that is related to a shear-induced (advective) Kelvin–Helmholtz instability. This aspect is discussed in the next section.

Figure 6 illustrates the effect of coflow velocity on the triple flame structure under 0 and 1 g conditions. The heat release rate contours are presented for following three cases: (a) $\phi_{in}=1.8$, $\phi_{out}=0.38$, $v_{in}=0.3$, $v_{out}=0.7$, $\phi_{overall}=0.5$; (b) $\phi_{in}=1.8$, $\phi_{out}=0.38$, $v_{in}=0.3$, $v_{out}=0.3$, $\phi_{overall}=0.63$; and (c) $\phi_{in}=1.8$, $\phi_{out}=0.38$, $v_{in}=0.3$, $v_{out}=0.1$, $\phi_{overall}=0.95$. The coflow velocity has a markedly different effect on the structures of the 0 and 1 g flames. For the 0 g flame, as v_{out} decreases, the advection in the outer stream is reduced and, consequently, the outer reaction zones move further away from the centerline. This increases the spatial separation between the nonpremixed zone and the outer premixed zone. This effect becomes more pronounced as v_{out} is reduced further. For the smallest coflow velocity, the outer premixed reaction zone becomes noticeably compact. This is caused by the significantly increased physical separation between the outer premixed zone and the central nonpremixed and inner premixed zones, which leads to reduced interaction between the two regions. In addition, the outer reaction zone becomes more stable as v_{out} is reduced at 0 g, an explanation for which is provided in the next section.

For the three cases shown in Fig. 6, the 0 g triple flame has a relatively stable behavior, whereas the corresponding 1 g flame exhibits a well-organized flicker of the outer reaction zone. Moreover, as the coflow velocity is decreased, the flickering becomes progressively more pronounced and causes oscillations in all three reaction zones. The flame flickering phenomena, whereby the flame is periodically pinched by a convecting vortex generated by the buoyancy-induced absolute instability, has been comprehensively discussed in previous experimental and computational studies.[10,14–17] However, in the cited studies, the flame flickering phenomena has been discussed in the context of either nonpremixed or premixed flames, but not with respect to a partially premixed triple flame.

The flickering frequency can be obtained by recording the temperature history at select spatial locations. Figure 7 presents these temperature history plots for the three 1 g flames depicted in Fig. 6. The plots indicate a well-organized flickering process for all three cases. For the case with high coflow velocity ($v_{out}=0.7$), the temperature oscillations have a relatively small amplitude ($\approx$6% of the maximum). Consequently, visual examination of the heat release rate contours for this case does not discern any perceptible flame flickering [cf. Fig. 6(a)]. However, for the other two cases with low coflow velocity, the temperature history plots show higher-amplitude oscillations and the flame flickering is prominent and immediately perceptible, which can be clearly inferred from the images in Figs. 6(b) and 6(c). Both the central nonpremixed and outer lean premixed zones flicker quite strongly, and their heights oscillate over a wide spatial range. For the third case ($v_{out}=0.1$), the magnitude of the oscillations is even more pronounced, and this large amplitude flicker in the outer zones also induces an oscillation in the inner premixed zone. This behavior attests to the fact that the three reaction zones are synergistically coupled and that the coupling is enhanced by transport effects (such as by buoyant advection in the presence of gravity).

The transient process and the relative amplitude of oscillations involved with flame flickering for the three cases are

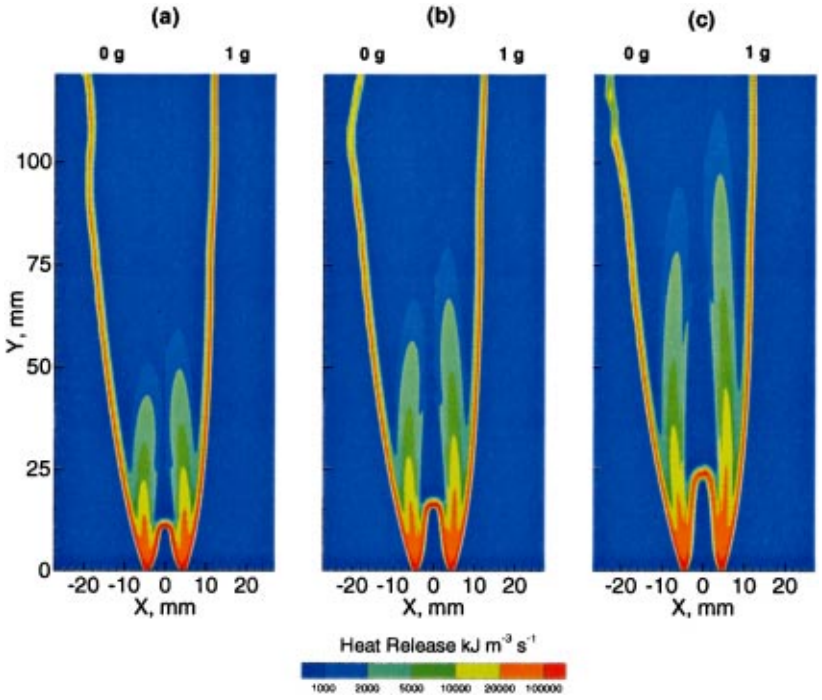

FIG. 5. Comparison of 0 g (left) and 1 g (right) triple flames in terms of the heat release rate (in units of $kJ\,m^{-3}\,s$) contours for three different stoichiometric and flow conditions: (a) $\phi_{in}=1.6$, $\phi_{out}=0.4$, $v_{in}=0.3\ m\,s^{-1}$, $v_{out}=0.7\ m\,s^{-1}$, $\phi_{overall}=0.5$; (b) $\phi_{in}=1.8$, $\phi_{out}=0.38$, $v_{in}=0.3\ m\,s^{-1}$, $v_{out}=0.7\ m\,s^{-1}$, $\phi_{overall}=0.5$; and (c) $\phi_{in}=2.1$, $\phi_{out}=0.36$, $v_{in}=0.3\ m\,s^{-1}$, $v_{out}=0.7\ m\,s^{-1}$, $\phi_{overall}=0.5$. Case (b) pertains to the reference flames.

more clearly depicted by the instantaneous images presented in Fig. 8. The three cases correspond to $v_{out}=0.7$, 0.3, and 0.1 $m\,s^{-1}$, respectively. For both predictions [and measurements presented in Fig. 8(d)], four images are shown within a single time period of oscillation. The images clearly show that there is a large amplitude flicker of both the central nonpremixed and outer lean premixed zones for the latter two cases. Their respective reaction zone heights oscillate over a wide spatial range. An oscillation is also observed in the inner premixed reaction zone for case (c), although the corresponding flicker amplitude is much smaller than that in the other two zones of the flame.

The buoyancy-induced instability is initiated at $Y \approx 30$ mm on the reactant side of the outer lean premixed flame. The resulting vortex convects downstream and strongly interacts with the lean premixed zone, thereby causing a large-amplitude flicker of this zone. This, in turn, induces a similar large-amplitude flicker in the nonpremixed reaction zone as its height oscillates over a wide spatial region. This coupling provides further evidence of the strong

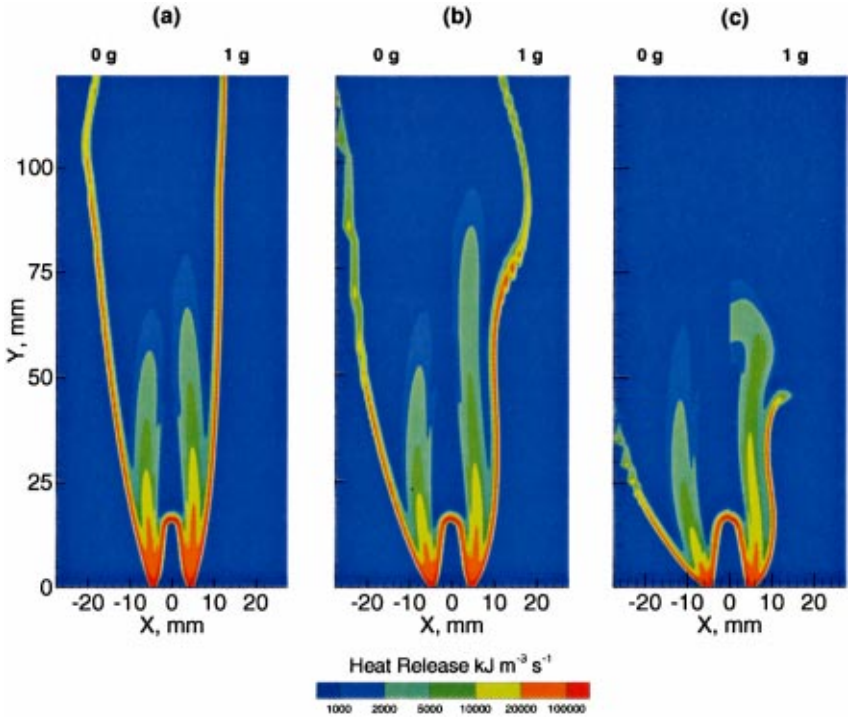

FIG. 6. Effect of coflow velocity on the triple flame structure under 0 and 1 g conditions. Heat release rate contours are shown for (a) $\phi_{in}=1.8$, $\phi_{out}=0.38$, $v_{in}=0.3\ m\,s^{-1}$, $v_{out}=0.7\ m\,s^{-1}$, $\phi_{overall}=0.5$, (b) $\phi_{in}=1.8$, $\phi_{out}=0.38$, $v_{in}=0.3\ m\,s^{-1}$, $v_{out}=0.3\ m\,s^{-1}$, $\phi_{overall}=0.63$, and (c) $\phi_{in}=1.8$, $\phi_{out}=0.38$, $v_{in}=0.3\ m\,s^{-1}$, $v_{out}=0.1\ m\,s^{-1}$, $\phi_{overall}=0.95$.

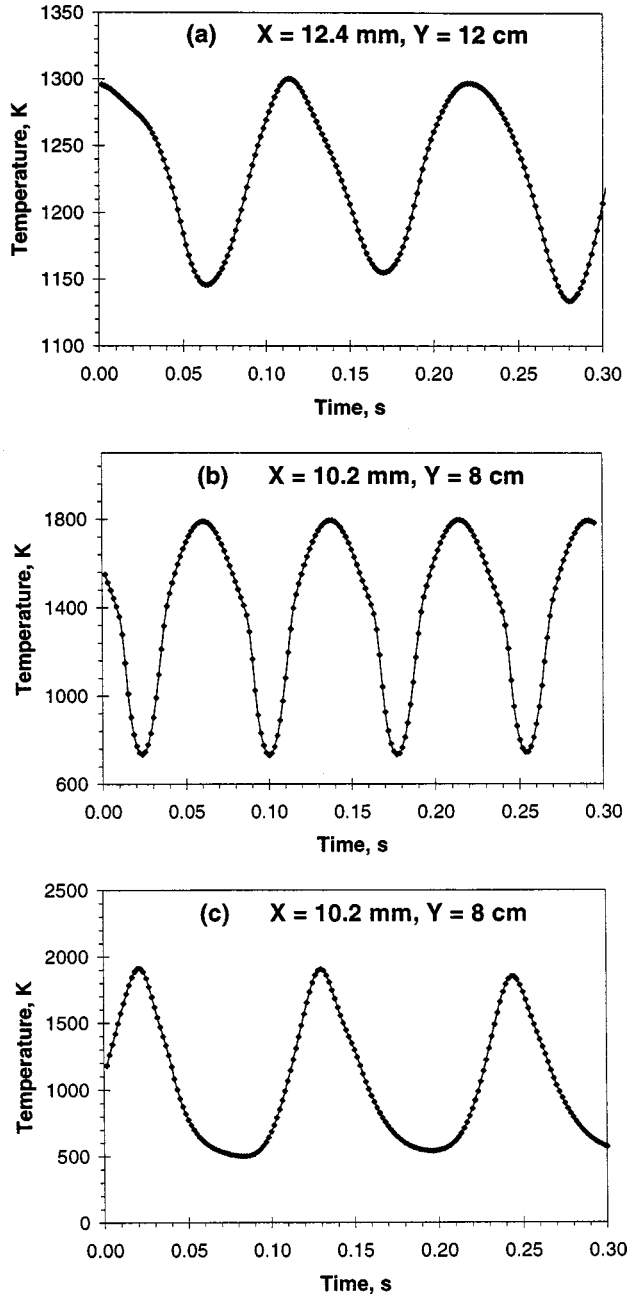

FIG. 7. Temperature history plots at selected spatial locations for the three 1 g flames discussed in the context of Fig. 6. The coflow velocities are: (a) $v_{out}=0.7\ m\ s^{-1}$, (b) $v_{out}=0.3\ m\ s^{-1}$, and (c) $v_{out}=0.1\ m\ s^{-1}$.

synergistic interactions between these two reaction zones. As the coflow velocity is reduced from 0.3 to 0.1 $m\,s^{-1}$, the flicker amplitude is further increased in both the lean premixed and nonpremixed zones. The increase in flicker amplitude is more clearly seen from the temperature-history plots presented in Fig. 7. At the lower coflow velocity of 0.1 $m\,s^{-1}$, the flicker of the nonpremixed zone is also accompanied by a periodic pinching of this zone, which can be inferred from the images presented in Fig. 8(c). Another important feature of flame-vortex interaction pertains to the unsteady curvature in the outer premixed zone that is induced by the convecting vortex. As the vortex moves downstream, it produces both convex and concave curvature in the lean premixed zone. This, in turn, induces a curvature in the nonpremixed reaction zone. The coupling of curvature and differential diffusion effects is known to influence radical production and flame dynamics during combustion.

High-speed video (Kodak) images were obtained for the flames established at the conditions corresponding to Figs. 8(b) and 8(c) at the rate of 250 frames s^{-1}. Assuming that the reaction zones correspond to locations of intense chemiluminescence, it is possible to observe the instantaneous topography of each reaction zone from the images. We have quantified the oscillations in the height of the inner premixed reaction zone, and the horizontal displacements of the nonpremixed and lean premixed reaction zones at a specified axial displacement. It is possible to characterize the oscillation frequency from these measurements. The oscillation frequencies were found to be identical using these three different criteria based on unsteadiness in each of the three reaction zones.

Figure 8(d) compares the high-speed video (flame luminescence) images (on the left) with the predicted heat release rates (on the right) for the case corresponding to $v_{out}=0.1$. A full oscillation period for this flame is $\approx$112 m s, and subsequent images correspond to every one-fourth of that cycle. Observing the figure from left to right, conspicuous changes in the flame structure are noticeable due to the unsteadiness. The first image depicts a high and relatively straight nonpremixed reaction zone, whereas the outer lean premixed reaction zone tends to diverge. The central nonpremixed and outer lean premixed zones subsequently narrow, and the inner reaction zone height becomes smaller. Finally, the outer reaction zone pinches off, reducing the heights of both the inner rich premixed and central nonpremixed reaction zones.

For the flames discussed in the context of Figs. 7 and 8, the flickering frequencies were obtained by using instantaneous video images as well as making temperature measurements using a thermocouple. While the thermocouple technique is unsuitable for making quantitative temperature measurements in these unsteady flames, it can nevertheless capture the temperature periodicity to yield the oscillation frequencies correctly. The measured and predicted frequencies are presented in Table I for the flames corresponding to Figs. 8(b) and 8(c). These are found to be in excellent agreement for both cases, and are, respectively, $\approx$12.2 and 8.8 Hz. The magnitude of the oscillations in the flame discussed in Fig. 8(a) are very small so that both thermocouple and video measurements in the laboratory flame are masked by noise.

While the amplitude of the oscillations exhibits a strong sensitivity to the change in the coflow velocity, the flickering frequency is weakly dependent on this velocity. For the three

TABLE I. Comparison between the predicted and measured frequencies (in Hz).

v_{out}, $m\,s^{-1}$	Predicted	Measured (high speed camera)	Measured (thermocouple)
0.3	12.5	12.2	12
0.1	8.8	8.9	8.7

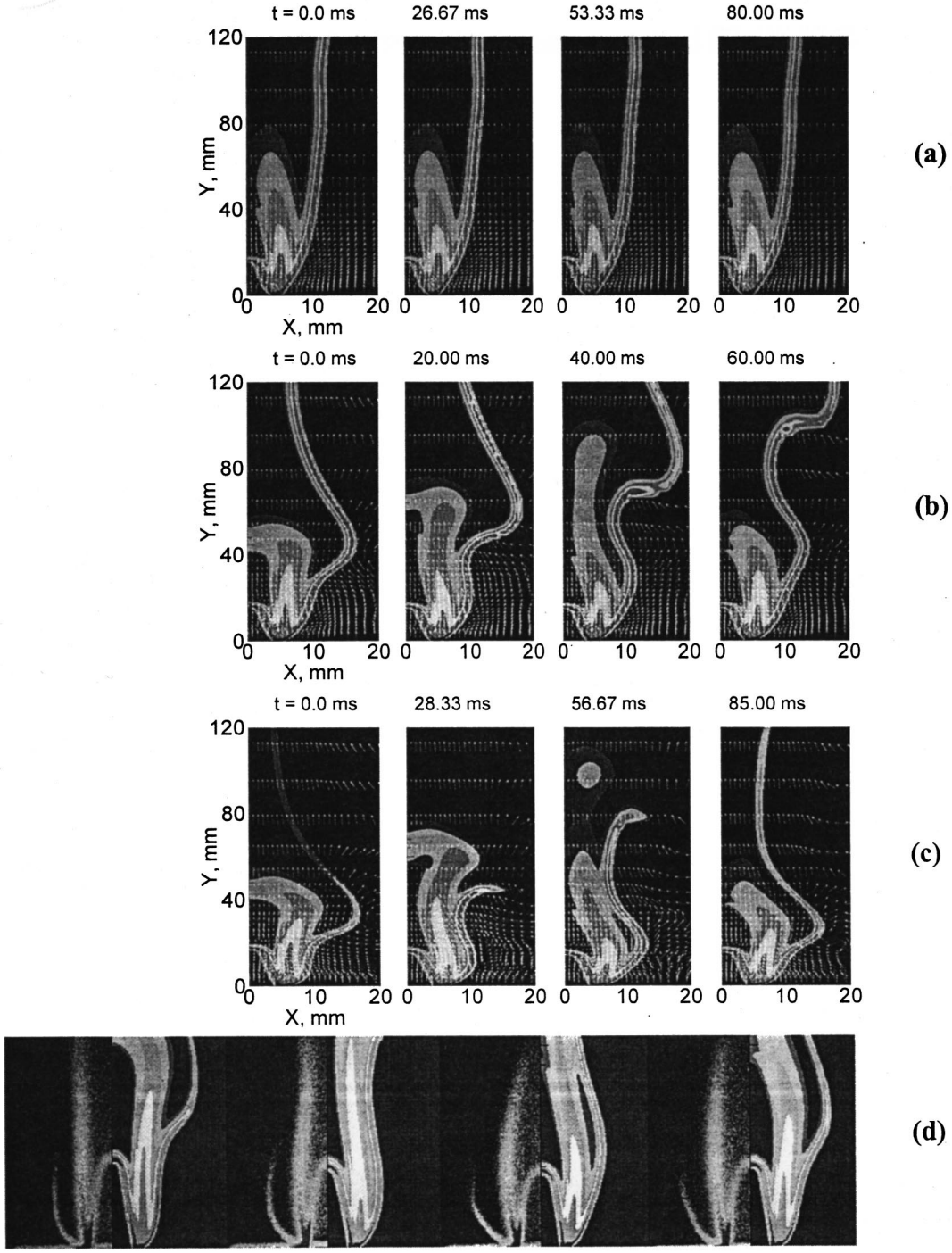

FIG. 8. Instantaneous images of the three 1 g flames (in the context of Fig. 6) at four different times within one period of oscillation. Each image contains heat release rate contours and velocity vectors. For case (c), the phase-matched predicted and measured (high-speed video) images at four different times are presented in Fig. 8(d).

cases illustrated in Fig. 7, the computed frequencies are 9.0, 12.2, and 8.8 Hz, respectively. (The temperature history was recorded at several spatial locations for each case and the reported frequencies were found to vary by less than two percent of these values.) The computed and measured frequencies are well within the range of experimental values reported for flickering nonpremixed (diffusion) flames.[14,17]

Presence of absolute and convective instabilities in triple flames

Our simulations have indicated the presence of either a shear-induced convective instability or a buoyancy-induced global instability in laminar triple flames, depending upon the magnitude of the coflow velocity and the gravitational acceleration. Evidence for this is provided by the heat release

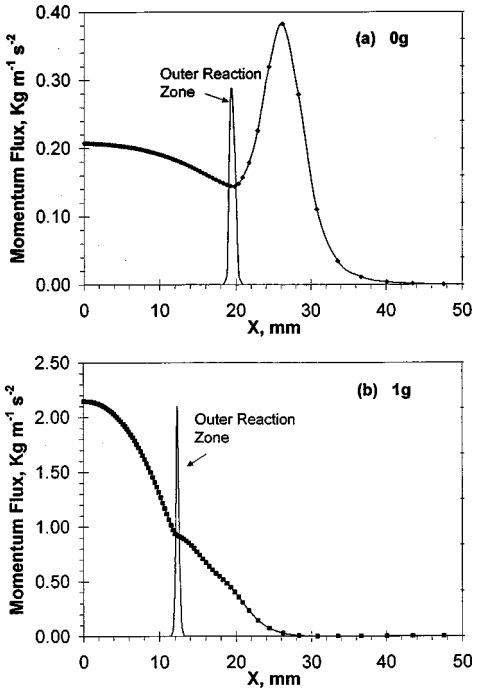

FIG. 9. Variation of momentum flux ρu^2 in the transverse direction for the 0 (a) and 1 g (b) reference flames that are discussed in the context of Fig. 3.

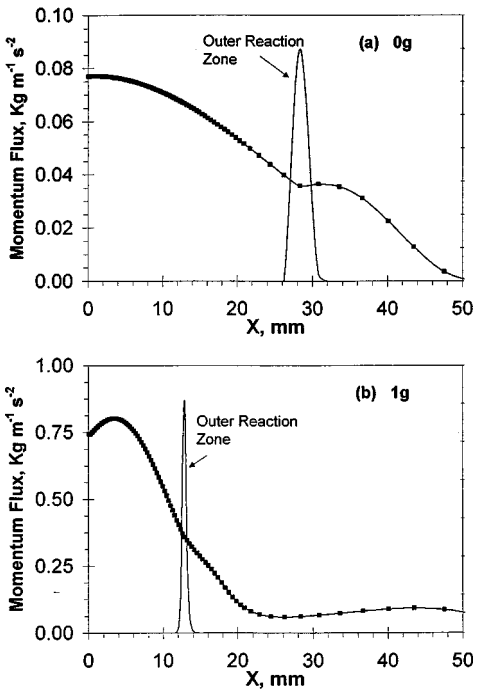

FIG. 10. Variation of momentum flux ρu^2 in the transverse direction for (a) 0 and (b) 1 g flames established at $\phi_{in}=1.8$, $\phi_{out}=0.38$, $v_{in}=0.3$, $v_{out}=0.3\ \mathrm{m\,s^{-1}}$, $\phi_{overall}=0.63$.

rate contours presented in Figs. 5 and 6. For the 1 g flame (cf. Fig. 6), as the coflow velocity is reduced from 0.7 to 0.3 $\mathrm{m\,s^{-1}}$, a large vortex structure is periodically generated due to the buoyancy-induced instability, which causes the outer premixed reaction zone to flicker. As the coflow velocity is further reduced, both the central nonpremixed and outer premixed zones strongly flicker, with their heights oscillating over a wide range. This also causes the inner premixed zone in the 1 g flame to oscillate. In contrast, decreasing the coflow velocity in the corresponding 0 g flames causes the outer reaction zones to become more stable. Flame flickering caused by buoyancy-induced convection has been extensively discussed in previous experimental, theoretical, and computational investigations.[10,14–20] However, the presence of a shear-induced instability in laminar triple flames under 0 g conditions has not been previously reported.

We will examine this aspect further. We present the transverse profiles of the axial momentum flux (ρu^2) for the 0 and 1 g reference flames in Fig. 9 at an axial displacement of $Y=120\,\mathrm{mm}$. The location of the outer reaction zone indicated in the figure is based on the important initiation reaction $CH_4+H\rightarrow CH_3+H_2$ that leads to subsequent fuel consumption. The outer lean premixed zone is located at $X\approx 20\,\mathrm{mm}$ for the 0 g flame and at $X\approx 12\,\mathrm{mm}$ for the 1 g flame. The momentum flux profile for the 0 g flame has a peak at $X\approx 27\,\mathrm{mm}$, which is followed by a shear layer that exists between $27<X<35\,\mathrm{mm}$. In the shear layer, the momentum flux drops sharply from its maximum value to zero. The existence of this shear layer for the 0 g case can be attributed to the combined effect of a relatively high coflow velocity and the absence of buoyancy.

The momentum flux in the region between the centerline and outer reaction zone is an order of magnitude higher for 1 g flame as compared to the 0 g flame. This difference occurs since the fluid acceleration in the 1 g flame is caused by both flow dilatation and buoyancy, whereas that in the 0 g flame is due to flow dilatation alone. The smaller momentum flux in the inner region is partly responsible for the peak in the momentum flux profile that occurs at $X\approx 27\,\mathrm{mm}$ in the 0 g flame. Additional factors contributing to the existence of this peak are (1) the higher coflow velocity, and (2) the increase in the mixture density which approaches its ambient value outside the lean premixed zone.

The frequency associated with the oscillation of the outer reaction zone is computed by recording the temperature history at selected spatial locations. The computed Strouhal number based on this frequency, a momentum thickness of 3 mm (defined by the distance over which the momentum flux decreases by 50%), and an average velocity of $0.5\ \mathrm{m\,s^{-1}}$ has a value of 0.027. For a constant density shear layer instability, the measured Strouhal number reported by Hussain and Hussain[21] is in the range from 0.025–0.031.

We hypothesize that the instability of the outer reaction zone in 0 g flame is a convective Kelvin–Helmholtz instability that occurs due to the existence of the momentum shear layer. It is important to note that this shear layer exists only when the coflow velocity is sufficiently high and the gravitational acceleration is zero. In order to provide additional validation for our hypothesis, results for another case are presented in Fig. 10. The coflow velocity has been reduced from 0.7 to $0.3\ \mathrm{m\,s^{-1}}$ for the flames discussed in Fig. 10, with the other conditions being the same as for the corresponding flames discussed in Fig. 9. For the smaller coflow velocity, the momentum flux for the 0 g case exhibits a rela-

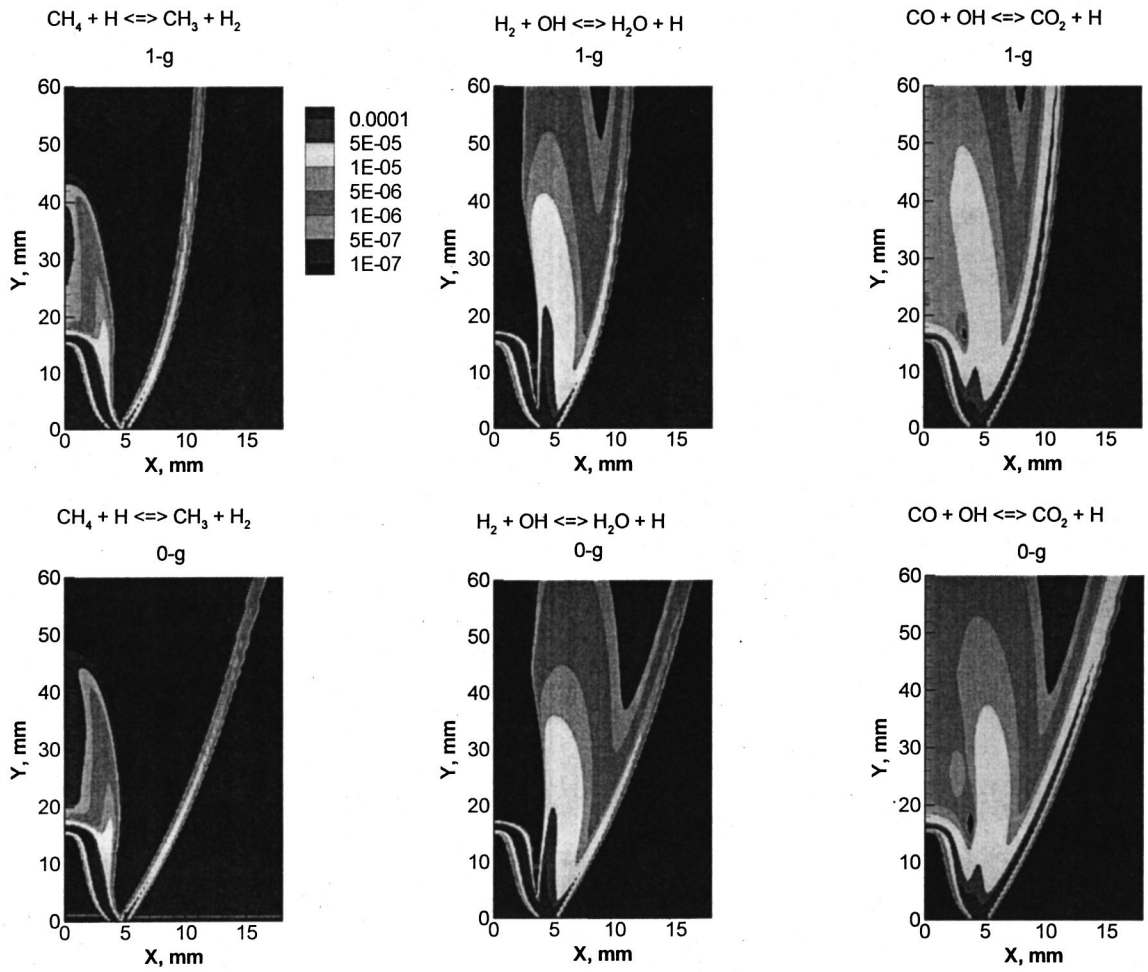

FIG. 11. Reaction rates contour plots for the reference flames for the reactions (a) $CH_4+H\Leftrightarrow CH_3+H_2$, (b) $H_2+OH\Leftrightarrow H_2O+H$, and (c) $CO+OH\Leftrightarrow CO_2+H$.

tively smooth profile indicating the absence of a distinct shear layer. Consequently, the outer reaction zone of the 0 g flame exhibits a relatively stable behavior [cf. Fig. 6(b)]. This was also confirmed by comparing the temperature history plots for the 0 and 1 g flames with $v_{\text{out}}=0.3\,\text{m s}^{-1}$. As noted earlier, the plots indicated a well-organized oscillatory behavior for the 1 g flame, but a steady-state behavior for the 0 g flame.

It is important to note that the gravitational effects on a partially premixed triple flame are different from those on a corresponding double flame.[7] Compared to a double flame, the nonpremixed reaction zone of a triple flame is relatively less affected by gravity. This difference is attributed to the presence of an outer lean premixed reaction zone in triple flames, which acts as a shield against the entrainment and enhanced advection caused by buoyancy. In addition, triple flames may be more prone to a buoyancy-induced instability, which leads to their well-organized flickering behavior. Our earlier investigation[7] dealing with the gravitational effects on partially premixed double flames essentially considered steady 0 and 1 g flames. The convective flow instability that we have simulated at 0 g in partially premixed flames has not been previously reported.

Effect of buoyancy on triple flame chemistry

The effect of buoyancy on the flame chemistry is illustrated in Fig. 11 in which we plot the reaction-rate contours of the major fuel decomposition reaction $CH_4+H\Leftrightarrow CH_3+H_2$, and the major product-formation reactions $H_2+OH\Leftrightarrow H_2O+H$ and $CO+OH\Leftrightarrow CO_2+H$ for the 1 (top) and 0 g (bottom) reference flames. The fuel decomposition reaction has similar strength in the inner rich premixed reaction zone for both the 0 and 1 g flames. However, it is relatively weaker in the central nonpremixed and outer lean premixed reaction zones of the 0 g flame than that at the corresponding locations in the 1 g flame. The larger separation between the central nonpremixed and outer premixed zones in the case of the 0 g flame is clearly illustrated by observing the fuel decomposition reaction rates. The rates of the reaction $H_2+OH\Leftrightarrow H_2O+H$ show that the central nonpremixed zone has a more open tip at 0 g, which permits a slightly larger leakage of H_2 through that reaction zone under that condition. The molecular hydrogen that leaks through the nonpremixed zone is consumed further downstream in the outer premixed reaction zone. The water formation reaction, which is significant in the nonpremixed and lean pre-

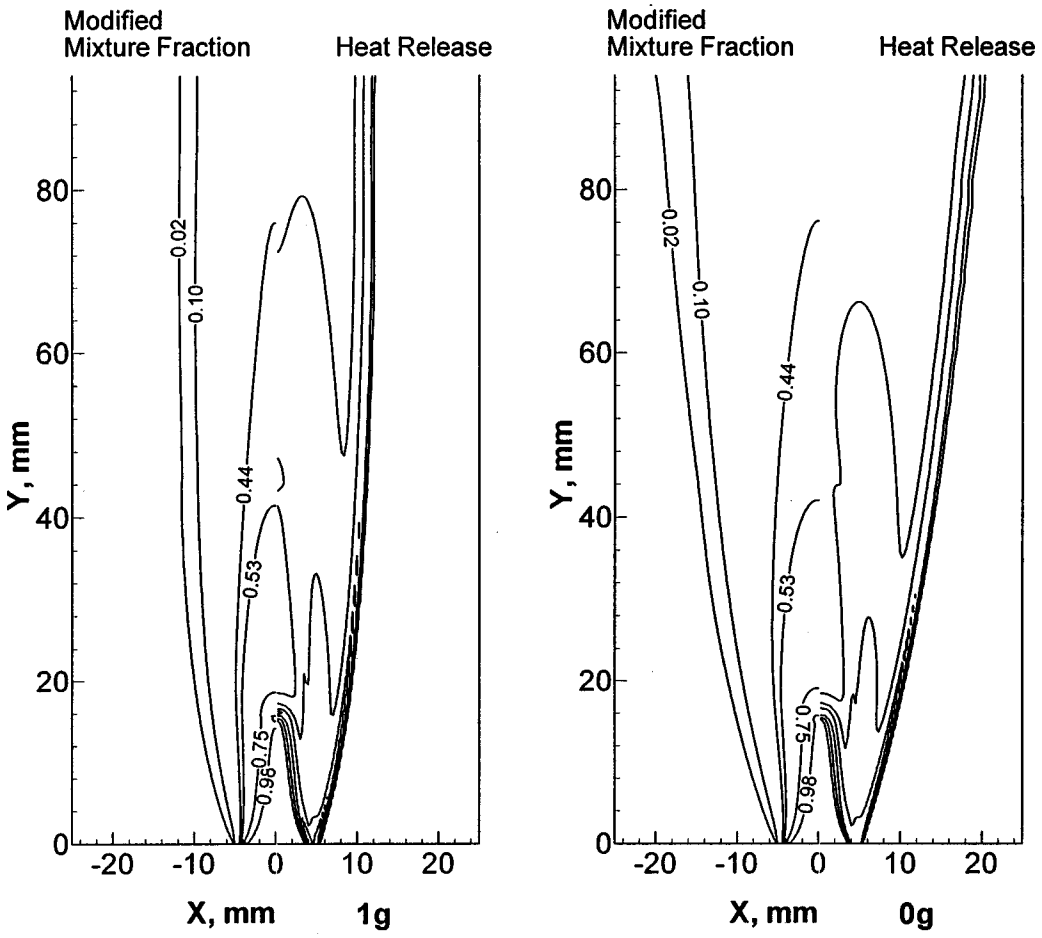

FIG. 12. Comparison of the 1 g and 0 g reference flames in terms of the modified mixture fraction and heat release rate contours.

mixed zones,[6] occurs in a broader region but at lower local rates at 0 g. Similar observations can be made regarding the CO-consumption reaction $CO+OH \Leftrightarrow CO_2+H$.

The triple flame structure and the interactions between the three reaction zones can be considered in terms of a modified conserved scalar ξ. We have found such an approach to be effective while characterizing the structure of an axisymmetric partially premixed flame.[2] A modified mixture fraction ξ can be defined on the basis of the elemental nitrogen mass fraction, i.e.,

$$\xi=(Z_{N,max}-Z_N)/(Z_{N,max}-Z_{N,min}),$$

where $Z_{N,max}$ denotes the elemental nitrogen mass fraction in the fuel-rich stream, Z_N the local mass fraction of elemental nitrogen, and $Z_{N,min}$ the corresponding mass fraction in the fuel-lean stream. Values of ξ are bounded by 0 (on the lean side) and 1 (on the rich side). Figure 12 presents the modified mixture fraction (left) and heat release rate (right) contours for the reference flames established at 1 and 0 g. The three reaction zones can be located by different contour ranges of ξ. For both cases, the inner rich premixed reaction zone lies between $0.75<\xi<0.98$, the central nonpremixed zone between $0.44<\xi<0.53$, and the outer lean premixed reaction zone lies between $0.02<\xi<0.10$, suggesting that the thermochemistry and state relationships are well-correlated in both cases.

Figure 13 presents the transverse profiles of temperature and the mass fractions of H, OH, and CO with respect to ξ at three axial displacements above the burner exit for the reference 0 and 1 g flames. The profiles at the lowest axial location (i.e., at 14 mm above the burner exit) include data from all three reaction zones. The axial displacement of 30 mm lies above the inner rich premixed reaction zone and, consequently, the profiles cross the central nonpremixed and the outer lean premixed reaction zones. Likewise, the data at a displacement of 75 mm cut across the outer lean premixed zone alone. The scalar profiles exhibit a gradient change at $\xi\approx0.3$ due to the existence of the outer lean premixed zone, at $\xi\approx0.55$ due to the central nonpremixed zone, and again at $\xi\approx0.8$ due to the outer rich premixed zone. The three reaction zones are also identified by presenting the heat release rate profile with respect to ξ for the 0 and 1 g flames. In general, the gradient changes in the scalar profiles occur at roughly at the same values of ξ, although these changes arise at different transverse locations in the physical space occupied by the two flames. The heat release rates for the two flames also exhibit a self-similar behavior. The results contained in Figs. 12 and 13 indicate the utility of the modified mixture fraction approach as a general tool to characterize the structure of laminar triple flames, regardless of the influence of buoyant transport.

The scalar profiles indicate that inner rich-premixed and

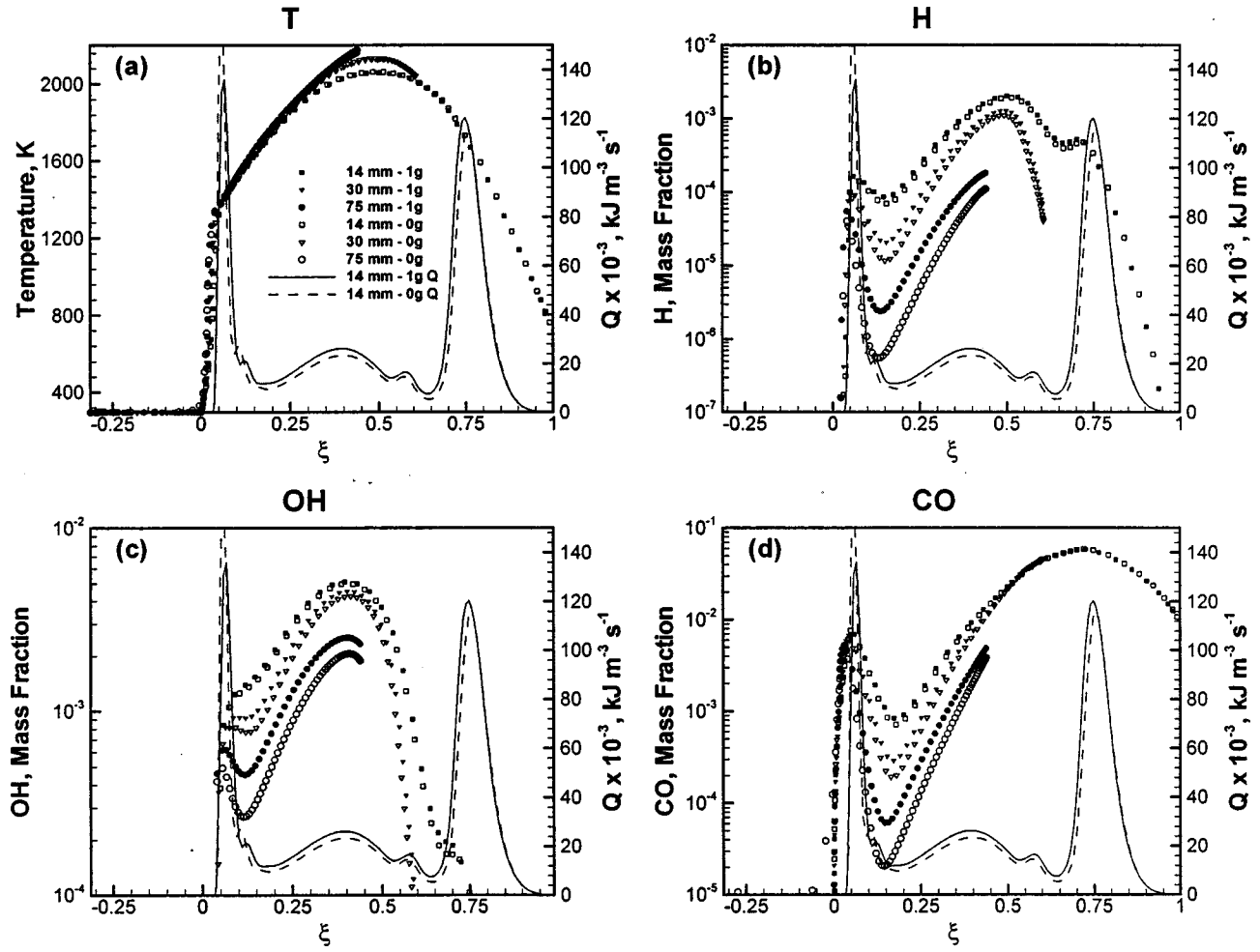

FIG. 13. Temperature and species (H, OH, CO) mass fraction profiles with respect to the modified mixture fraction for the reference flames.

central nonpremixed reaction zones are relatively uninfluenced by gravity. However, the scalar profiles in the lean premixed reaction zones are noticeably different at 0 and 1 g. In general, at lower axial displacements the radical (H and OH) species' mass fractions are smaller for the 0 g flame than those for the 1 g flame. This arises due to the reduced interaction between this and the central nonpremixed zone that leads to a lower chemical activity in the lean premixed zone of the 0 g flame. As has been previously discussed, the larger physical separation between the two zones is a consequence of the reduction in advective transport.

The mass fraction profiles with respect to the modified mixture fraction provide useful insight regarding scalar transport and the synergistic interactions between the reaction zones. For instance, these profiles indicate that the maxima in the radical species concentrations occur in the nonpremixed reaction zone. This implies that the nonpremixed zone represents a region of higher chemical activity from which H-atoms and OH radicals are transported to the two premixed reaction zones. This phenomena is also illustrated for the reference flames through Figs. 14 and 15, which, respectively, present the advective and diffusive fluxes of H-atoms and other species. The nonpremixed zone, being the region of highest temperature, also provides heat to both premixed zones. The maximum in the CO mass fraction occurs in the rich premixed zone, indicating that CO is largely produced there and subsequently transported to the nonpremixed zone where it is converted into CO_2. Similar observations can be made regarding H_2.

Figure 13 also indicates that the chemical structures of the rich and lean premixed zones are markedly different. The hydroxyl mass fraction drops sharply in the region between the nonpremixed and rich premixed reaction zones, implying that the OH radicals are both produced and consumed in the nonpremixed zone, as well as transported to the inner and outer premixed zones. The mass fraction of radical species in the nonpremixed and lean premixed regions decrease in the downstream direction as these species approach their equilibrium concentrations and are diluted by the transport of air.

Species advection and diffusion in 1 g and 0 g triple flames

Figure 14 presents the advective fluxes of CH_4, O_2, and H-atoms for the 0 and 1 g flames. The advection flux is defined as $\rho\, Y_i\, \mathbf{V}$ where ρ is the mixture density, Y_i the concentration of the *i*-species, and $\mathbf{V}$ the velocity. The figure also contains the heat release rate contours to differentiate the three reaction zones. The advection of methane and oxygen into the inner flame is generally similar for the two

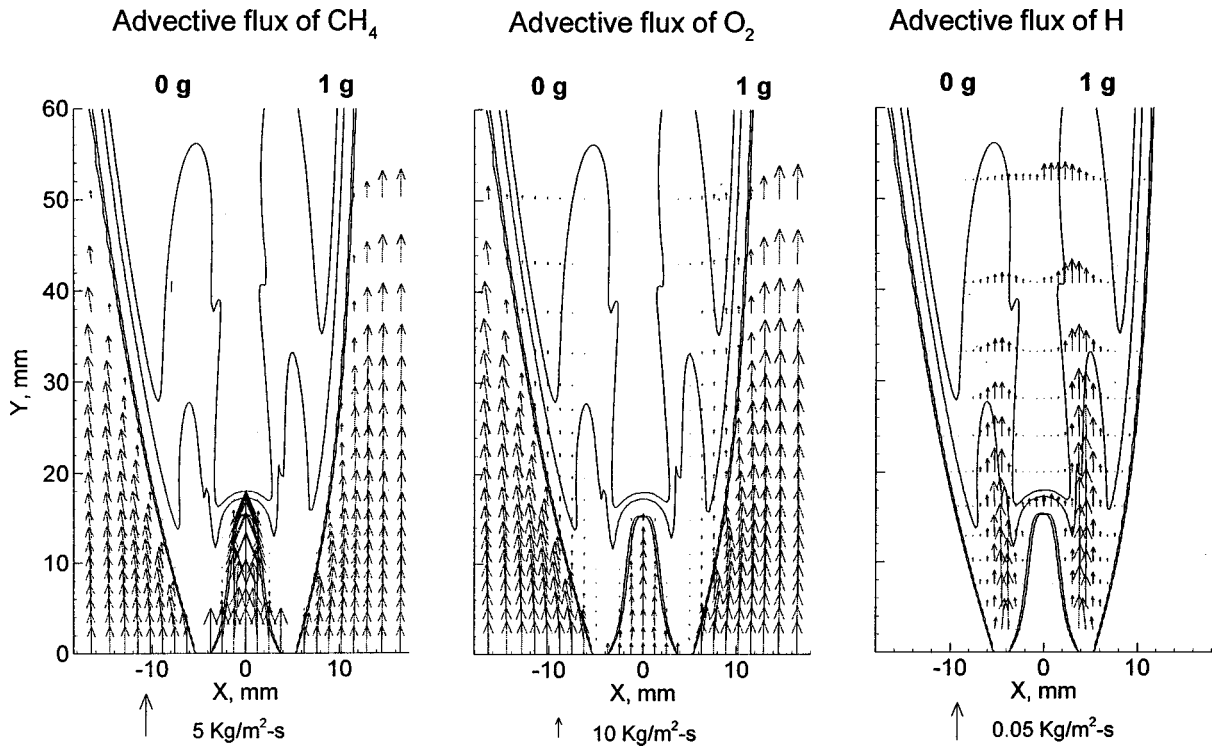

FIG. 14. Comparison of the advective fluxes of CH_4, O_2, H for the 0 g (left) and 1 g (right) reference flames.

flames, since this is dominated by the fluxes introduced into the burner. However, in the region upstream of the lean premixed zone, the advection of these species differs significantly in the two flames. At 0 g, the direction of advection is directed further away from the centerline, since entrainment diminishes in the absence of buoyant convection. Consequently, the physical separation between the nonpremixed and lean premixed zones increases at 0 g. The advection of H-atoms mostly occurs in the nonpremixed zone, which indicates their availability in this region. The advective flux of

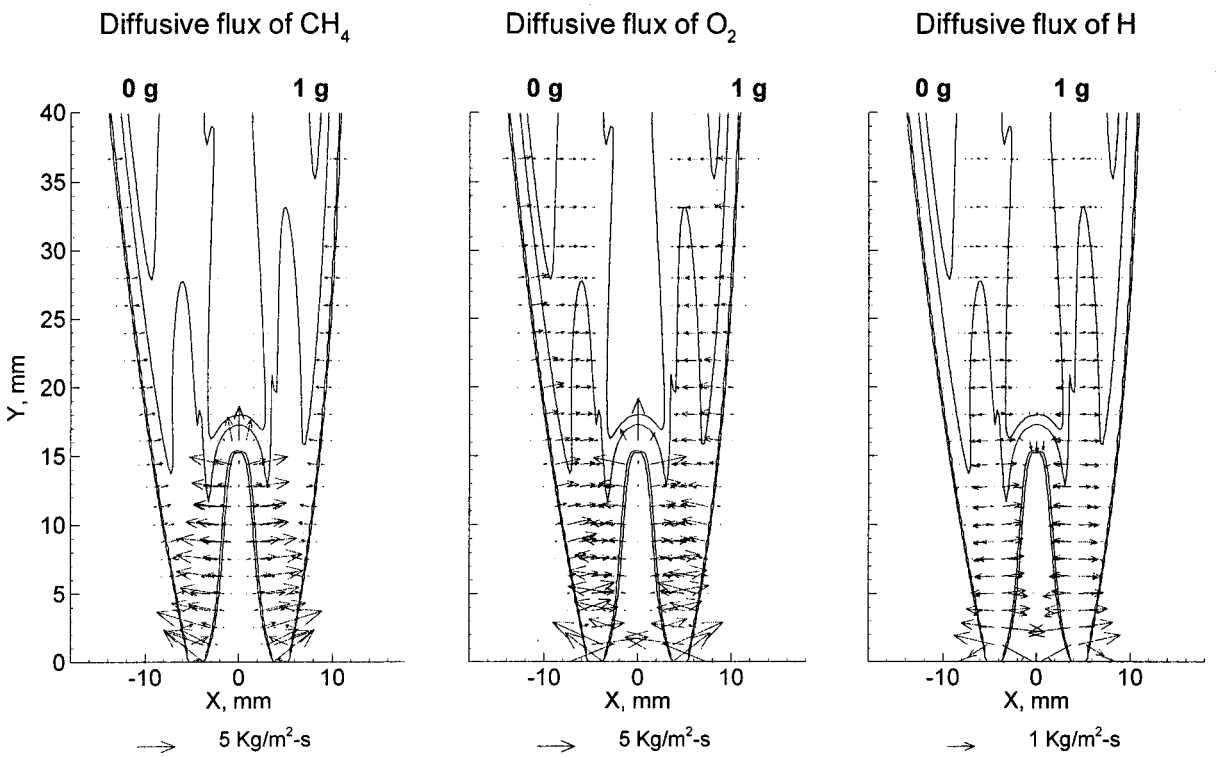

FIG. 15. Comparison of the diffusive fluxes of CH_4, O_2, H for the 0 g (left) and 1 g (right) reference flames.

H-atoms is significantly enhanced by gravity, which leads to an increase in the height of the nonpremixed reaction zone at 1 g. The advective flux of H is directed toward the centerline due to buoyancy and, therefore, the 1 g flame is more compact than the corresponding 0 g flame.

The diffusive fluxes of CH_4, O_2, and H [defined as $-\rho D_{i-N_2}(\partial Y_i/\partial x)\mathbf{i}-\rho D_{i-N_2}(\partial Y_i/\partial y)\mathbf{j}$] are presented in Fig. 15 for the 0 and 1 g flames. The diffusive flux of CH_4 indicates leakage of methane from the inner premixed zone to the nonpremixed zone, while that of O_2 indicates diffusion of this species from both the rich and lean premixed zones toward the nonpremixed zone. The diffusive flux of H-atoms indicates that H is produced in the nonpremixed reaction zone and is then transported to both the inner and outer premixed zones.

No significant differences related to diffusive transport are observed for the two flames in either of the three reaction zones, although there is slightly higher diffusion in the nonpremixed and lean premixed zones at 1 g. Buoyancy influences diffusive fluxes in a less direct manner than it does advection. The 0 g flame exhibits generally broader nonpremixed and lean premixed reaction zones. Consequently, the species concentration gradients in this flame are less steep than in the 1 g flame, which lowers the diffusive transport. Overall, diffusion is not as greatly influenced by gravity as is advection, although its importance relative to advection is enhanced at 0 g. The decrease in both diffusion and advection at 0 g results in a flame that is less compact and has thicker reaction zones, and which, therefore, is more sensitive to flow or stoichiometry perturbations.

Thermal radiation effects

We have not considered thermal radiation effects in this investigation. The high-temperature regions are much broader at 0 g and, consequently, thermal radiation effects can become significant as the role of gravity is diminished. The radiative cooling time τ_r for a gaseous volume of combustion products that is initially at its adiabatic flame temperature T_f is $\tau_r = T_f/(dT/dt) \approx T_f/(q/\rho c_p)$, where q denotes the heat loss rate, ρ the density, and c_p the specific heat at constant pressure.[7,22] The optically thin gas assumption implies that $q=(4\sigma a_p(T_f^4-T_0^4))$, where σ represents the Stefan–Boltzmann constant, a_p the Planck mean absorption coefficient, and T_0 the ambient temperature. Using the ideal gas state relation and the expression for q, $\tau_r \approx (\gamma/(\gamma-1))P/(4\sigma a_p(T_f^4-T_0^4))$, where γ denotes the specific heat ratio, and P is the ambient pressure. Assuming $P=1$ atm, $a_p = 56\,\mathrm{cm}^{-1}$, $\gamma=1.35$, $T_0 = 298$ K, and the partially premixed ''flame'' temperatures to vary from 1650 to 2200 K (in the inner premixed and outer nonpremixed reaction zones), the corresponding τ_r values lie in the range 0.3–0.09 s.

The diffusive transport time scale $\tau_d = \delta^2/\alpha$, where δ denotes a transport zone thickness and α a temperature-averaged diffusivity. The buoyant transport time scale $\tau_b \approx L/U_b$, where, L represents a characteristic length, $U_b \approx (gL(\Delta\rho/\rho))^{1/2}$ is the buoyancy-induced velocity, and $\Delta\rho$ denotes the density change across the reaction front. In general, $\Delta\rho/\rho \approx 1$, so that $\tau_b \approx (L/g)^{1/2}$.[22] Representative values for α and g, respectively, are taken to be 1.5 and 980 $\mathrm{cm\,s}^{-2}$. For $1 \leqslant L \leqslant 10$ cm, τ_b varies from 0.03 to 0.1 s. For τ_d to lie within these bounds, $\delta = 2$–4 mm. This thickness depends on the level of partial premixing and the velocities of the reactant streams. Therefore, if the transport zone thickness exceeds 4 mm (as is the norm in the flames that we have investigated, as illustrated in Figs. 14 and 15), $\tau_b < \tau_d$, i.e., gravitational effects overwhelm transport effects.

Radiation effects are relatively unimportant at normal gravity, since $\tau_b < \tau_r$. However, $\tau_b \to \infty$ as $g \to 0$, and radiation effects can be significant under microgravity conditions. As $g \to 0$ we have shown that the role of molecular transport becomes more important, and it is possible that $\tau_r \approx \tau_d$. Therefore, future investigations should address the issue of thermal radiation effects.

CONCLUSIONS

We have presented the results of a detailed investigation on the effects of buoyancy on the structure of laminar methane–air triple flames established on a Wolfhard–Parker slot burner. The computations have been validated by comparing the measured and predicted velocity fields, and the experimentally obtained chemiluminescent C_2^* emission with the spatial distribution of predicted heat release rates for a representative triple flame established at a near-unity Froude number. The flickering frequencies of the 1 g triple flames obtained from simulations and measurements are also found to be in good agreement. Numerical results are then used to characterize the effects of equivalence ratio and coflow velocity on the structure of 0 g and 1 g triple flames. Important observations are as follows:

(1) Combustion occurs in three reaction zones: An inner rich premixed zone, a central nonpremixed zone, and an outer lean premixed zone. The central nonpremixed reaction zone is established in the region where ''fuel'' and ''oxidizer'' supplied from the respective rich and lean premixed reaction zones mix in stoichiometric proportion. The overall flame structure is determined by the interactions that occur between the three reaction zones, and can be controlled by changing the mixture velocity, equivalence ratio, and gravitational acceleration.
(2) The inner premixed zone consumes CH_4 and O_2, and supplies CO, H_2 (the ''intermediate fuels'' for the nonpremixed reaction zone) and excess methane to the nonpremixed zone. The nonpremixed zone consumes these fuels and, in turn, produces radical species such as OH and H-atoms that are transported to the inner and outer premixed zones and consumed there. The outer zone provides oxygen to the nonpremixed zone. The nonpremixed zone, being the region of highest temperature, also provides heat to both premixed zones.
(3) For all the conditions investigated, the zero-g flame is spatially larger than the corresponding normal-gravity flame, since the physical separation between the three reaction zones is significantly increased in the absence of gravity. This can be attributed to two factors. First, the entrainment into the outer premixed and nonpremixed

reaction zones is reduced due to the absence of buoyancy. Second, the buoyancy-induced advection downstream of the inner premixed and nonpremixed reaction zones is absent, while the flow dilatation effects in these regions push both the nonpremixed and outer premixed zones away from the centerline.

(4) While the spatial characteristics of the inner premixed zone are relatively unaffected by gravity, both the nonpremixed and outer premixed reaction zones exhibit significant differences under 0 and 1 g conditions. For 0 g flames, the central nonpremixed and outer premixed zones are located farther away from the centerline compared to those in the corresponding 1 g flames. In addition, the 0 g nonpremixed reaction zone is less stretched due to reduced upstream advection, and less intense (through a reduced chemical activity as a consequence of lower mass transport) at its tip. The absence of gravity also decreases the central reaction zone height, since the residence time is increased.

(5) A fundamental difference between the 0 and 1 g triple flame is due to their markedly different response to a change in the coflow velocity. For 0 g flames, as the coflow velocity is reduced, the outer premixed zone moves farther away from the centerline, since advection in the outer stream is reduced. This increases the physical separation and, thus, results in a decreased interaction between the reaction zones at 0 g. This effect becomes increasingly more pronounced as the coflow velocity is further reduced. In contrast, decreasing the coflow velocity in 1 g flames leads to a reduced spatial separation and, thus, a stronger interaction between the reaction zones.

(6) The stability of 0 and 1 g laminar triple flames is significantly different. While a 0 g flame exhibits an oscillatory behavior only under high coflow velocity conditions, a corresponding 1 g flame almost always flickers. The flame flickering at 1 g is due to a buoyancy-induced absolute instability that is more pronounced and better organized as the coflow velocity is decreased. In contrast, the oscillations in the 0 g flame are caused by a convective Kelvin–Helmholtz type instability of the momentum shear layer that disappears as the coflow velocity is decreased.

(7) Although the flickering at 1 g is initiated in the outer premixed zone, it is not confined to this zone. As coflow velocity is reduced, the flickering becomes stronger, more organized, and causes oscillations in all three reaction zones. Both the computed and measured frequencies are found to be in a narrow range extending from 9 to 12 Hz, in accord with previous experimental and computational studies dealing with flickering nonpremixed flames. In contrast, the instability in the 0 g flames is confined to the outer premixed zone. The computed Strouhal number for the 0 g oscillations is 0.027, which is in accord with that for constant density shear layers (that lies in the range 0.025–0.031).

(8) There is good agreement between the predicted and measured (high-speed video) dynamics of the flickering 1 g flame. In addition, the predicted flickering frequency is found to be in excellent agreement with that obtained from temperature measurements as well as from high-speed video images.

(9) The modified conserved scalar approach is found to be an effective tool to characterize the structure of partially premixed triple flames under both 1 g and 0 g conditions. The mass fraction profiles in terms of the modified mixture fraction indicate that the inner rich-premixed and central nonpremixed reaction zones are relatively uninfluenced by gravity. However, the scalar profiles in the lean premixed reaction zones are noticeably different at 0 and 1 g. In general, the radical (H and OH) species' mass fractions are smaller for the 0 g flame than those for the 1 g flame. This arises due to the reduced interaction between this and the central nonpremixed zone that leads to a lower chemical activity in the lean premixed zone of the 0 g flames.

(10) Gravitational effects on a partially premixed triple flame are different from those on a corresponding double flame. Compared to a double flame, the nonpremixed reaction zone of a triple flame is relatively less affected by gravity. This difference is attributed to the presence of an outer lean premixed reaction zone in triple flames, which acts as a shield against the entrainment and enhanced advection caused by buoyancy. In addition, triple flames appear to be more prone to a buoyancy-induced instability, which leads to their well-organized flickering behavior.

ACKNOWLEDGMENTS

This research was supported by the National Science Foundation Combustion and Plasma Systems Program through Grant No. CTS-9707000 for which Dr. Farley Fisher is the Program Director. Simulations were performed on the SGI workstations at NCSA at Urbana-Champaign. Many fruitful discussions with Dr. V. R. Katta of ISSI are greatly appreciated. Contributions of Z. Shu in running the computer code and of Phillip J. Erisman in image processing are acknowledged.

[1] Z. Shu, S. K. Aggarwal, V. R. Katta, and I. K. Puri, ''A numerical investigation of the flame structure of an unsteady inverse partially-premixed flame,'' Combust. Flame **111**, 296 (1997).

[2] S. K. Aggarwal and I. K. Puri, ''Flame structure interactions and state relationships in an unsteady partially-premixed flame,'' AIAA J. **36**, 1190 (1998).

[3] Z. Shu, B. J. Krass, C. W. Choi, S. K. Aggarwal, V. R. Katta, and I. K. Puri, ''Investigation of the flame structure of a steady two-dimensional partially-premixed methane-air flame,'' *Twenty-seventh Symposium (International) on Combustion* (The Combustion Institute, 1998), pp. 625–632.

[4] G. R. Ruetsch, L. Vervisch, and A. Liñán, ''Effects of heat release on triple flames,'' Phys. Fluids **7**, 6 (1995).

[5] P. N. Kioni, B. Rogg, K. N. C. Bray, and A. Liñán, ''Flame spread in laminar mixing layers: the triple flame,'' Combust. Flame **95**, 276 (1993).

[6] R. Azzoni, S. Ratti, S. K. Aggarwal, and I. K. Puri, ''The structure of triple flames stabilized on a slot burner,'' Combust. Flame **119**, 23 (1999). Also presented at the 34th AIAA/ASME/SAE/ASEE Joint Propulsion Conference, Cleveland, OH, July 13–15, 1998.

[7] Z. Shu, C. W. Choi, S. K. Aggarwal, V. R. Katta, and I. K. Puri, ''Gravity effects on steady two-dimensional partially-premixed methane-air flames,'' Combust. Flame **118**, 91 (1999).

[8]V. R. Katta, L. P. Goss, and W. M. Roquemore, ''Effect of nonunity Lewis number and finite-rate chemistry on the dynamics of a hydrogen-air jet diffusion flame,'' Combust. Flame **96**, 60 (1994).
[9]N. Peters, in *Reduced Kinetic Mechanisms for Applications in Combustion Systems*, *Lecture Notes in Physics*, edited by N. Peters and B. Rogg (Springer-Verlag, New York, 1993, Vol. M15, pp. 3–14.
[10]V. R. Katta, L. P. Goss, and W. M. Roquemore, ''Numerical investigations of transitional H_2/N_2 Jet Diffusion Flames,'' AIAA J. **32**, 84 (1994).
[11]K. McManus, B. Yip, and S. Candel, ''Emission and laser-induced fluorescence imaging methods in experimental combustion,'' Exp. Therm. Fluid Sci. **10**, 486 (1995).
[12]R. W. B. Pearse and A. G. Gaydon, *The Identification of Molecular Spectra*, 4th ed. (Chapman and Hall, London, 1976), p. 83.
[13]H. N. Najm, P. H. Paul, C. J. Mueller, and P. S. Wyckoff, ''On the adequacy of certain experimental observables as measurements of flame burning rate,'' Combust. Flame **113**, 312 (1998).
[14]J. Buckmaster and N. Peters, ''The infinite candle and its stability-a paradigm for flickering diffusion flames,'' *Twenty-First Symposium (International) on Combusion* (The Combustion Institute, Pittsburgh, 1986), pp. 1829–1836.
[15]R. W. Davis, E. F. Moore, W. M. Roquemore, L. D. Chen, V. Vilimpoc, and L. P. Goss, ''Preliminary results of a numerical-experimental study of the dynamic structure of a buoyant jet diffusion flame,'' Combust. Flame **83**, 263 (1991).
[16]J. L. Ellzey and E. S. Oran, ''Effects of heat release and gravity on an unsteady diffusion flame,'' in *Twenty-Third Symposium (International) on Combustion* (The Combustion Institute, Pittsburgh, 1992), p. 1635.
[17]T. Yuan, D. Durox, and E. Villermaux, ''An analog study for flame flickering,'' Exp. Fluids **17**, 104 (1994).
[18]P. A. Monkewitz and K. D. Sohn, ''Absolute instability in hot jets,'' AIAA J. **26**, 911 (1988).
[19]S. Ragu and P. A. Monkewitz, ''The bifurcation of a hot round jet to limit-cycle oscillations,'' Phys. Fluids A **3**, 501 (1991).
[20]J. S. Turner, *Buoyancy Effects in Fluids* (Cambridge University Press, Cambridge, 1973, p. 94.
[21]Z. D. Hussain and A. K. M. F. Hussain, ''Natural instability of free shear layers,'' AIAA J. **21**, 1512 (1983).
[22]P. D. Ronney, ''Combustion Experiments in Space'' Invited paper presented at the 36th Israel Annual Conference on Aerosciences, February 1996.